Computers in Biology and Medicine 111 (2019) 103338

Contents lists available at ScienceDirect

Computers in Biology and Medicine

journal homepage: www.elsevier.com/locate/compbiomed

Stent-induced vessel deformation after intracranial aneurysm treatment – A hemodynamic pilot study

Samuel Voß[a,b,*], Oliver Beuing[a,c], Gábor Janiga[a,b], Philipp Berg[a,b]

[a] Forschungscampus STIMULATE, University of Magdeburg, Sandtorstraße 23, 39106, Magdeburg, Germany
[b] Department of Fluid Dynamics and Technical Flows, University of Magdeburg, Universitaetsplatz 2, 39106, Magdeburg, Germany
[c] Department of Neuroradiology, University Hospital Magdeburg, Leipziger Str. 44, 39120 Magdeburg, Germany

ARTICLE INFO

Keywords:
Intracranial aneurysm
Vascular deformation
Stenting
Coiling
Hemodynamics
Computational fluid dynamics

ABSTRACT

Background: Stent-assisted coiling has become an important treatment option for intracranial aneurysms. However, studies have shown that this procedure can lead to the deformation of the local vasculature. Its effect on intra-aneurysmal hemodynamics still remains unclear.
Methods: Pre- and post-interventional image data of three representative middle cerebral artery aneurysms are considered in this study. This includes virtually deployed stents and coils. To evaluate the proportional effect of a) vessel deformation, b) stent deployment, and c) coil placement, 24 unsteady blood flow simulations were carried out focusing on the separated effects related to intra-aneurysmal hemodynamics. Four flow parameters (velocity within the aneurysm sac, aneurysm neck inflow rate, inflow concentration index, and ostium inflow area) and four shear parameters (wall shear stress, normalized wall shear stress, shear concentration index, and high shear area) were quantified.
Results: All of the considered flow and shear parameters, except for the shear concentration index, were clearly reduced due to treatment. Coiling and stenting caused a distinct and smaller neck inflow rate, respectively, while the impact of deformation was inconsistent among the aneurysms. Overall, coiling appears to have the strongest impact on local hemodynamics.
Conclusion: Stent-induced vessel deformation has a clear impact on intra-aneurysmal hemodynamics. This effect is neglected by the majority of previous studies, which consider the pre-interventional state for investigating the relation of stents and hemodynamics. The findings of this pilot study suggest that while stent-assisted coiling can lead to an improved hemodynamic situation, undesired flow conditions may occur in response to treatment.

1. Introduction

Stent-assisted coiling has become a frequently used, minimally invasive treatment method for intracranial aneurysms, especially in the case of incidental aneurysms [1–4]. In recent years, observations of stent-induced modifications of the cerebral vascular anatomy related to stent-assisted coiling therapy have been reported [5–10]. In these studies, pre- and post-interventional 2D or 3D angiography was used to quantify the grade of deformation.

Additionally, King et al. [9] performed image segmentation and centerline extraction to improve the measurement accuracy. This led to the finding that on average, the curvature radius increased by more than 50% after stent implantation, independent of the considered locations and coil packing within the associated aneurysm.

However, other studies found that stent-induced anatomical deformations are more likely to occur in distal locations compared to proximal locations of the cerebral vasculature [6,7]. Here, a presence of deformation is observed in 93% of the middle cerebral artery (MCA) aneurysms and 85% of the anterior communicating artery aneurysms after the implantation of a Leo stent (Balt, Montmorency, France) [6]. In addition, Gao et al. [7] correlated the stent design with the deformation grade. Thus, a higher bending stiffness of stents with closed-cell designs is more likely to cause anatomical deformations.

Until now, it is not clear how the observed vessel deformations influence the outcome of the therapy, and whether or not the change of local hemodynamics has a negligible impact on the therapy. Therefore, several studies have focused on the hemodynamics of treated intracranial aneurysms using Computational Fluid Dynamics (CFD) [11–14].

Gao et al. [15,16] virtually removed the aneurysms from the parent

* Corresponding author. University of Magdeburg, Universitaetsplatz 2, 39106, Magdeburg, Germany.
E-mail address: samuel.voss@ovgu.de (S. Voß).

https://doi.org/10.1016/j.compbiomed.2019.103338
Received 13 February 2019; Received in revised form 18 June 2019; Accepted 18 June 2019
0010-4825/

arteries prior to the actual CFD simulation. They found a decreased pressure drop at the bifurcation apex and a migration of the flow impingement zone due to vessel modifications. In another study, Jeong et al. [17] investigated two idealized bifurcation aneurysms, as well as stents and coils (modeled as porous media). They demonstrated that vessel straightening caused a decrease of mean velocity, kinetic energy, wall shear stress (WSS), and vorticity. In a more realistic approach, Voss et al. [18] examined patient-specific vessel geometry and aneurysm morphology in a pilot study. In this case, the isolated effect of vessel deformation resulted in a neck inflow rate reduction of 52.5%. In contrast, Kono et al. [19] found that in 16 sidewall aneurysms with only moderate deformation, the stent struts lead to higher flow reduction compared to the deformed geometry (23.1% vs. 9.6%).

Overall, the existing literature related to treatment-induced vessel deformations reveals that the relevant phenomena that occur may have an impact on the individual therapy outcome. However, these effects are rather sparsely documented and there is a certain need for an improved understanding of the corresponding causes. In this pilot study, the authors focus on a clear separation of the effects related to intra-aneurysmal hemodynamics for three treated MCA bifurcation aneurysms. Specifically, a) stent-induced vessel **deformation**, b) virtual **stenting**, and c) virtual **coiling** were investigated as single and combined factors affecting aneurysmal flow and shear parameters. Thus, this study allows for a quantification of each parameter in order to evaluate the individual importance regarding flow modification.

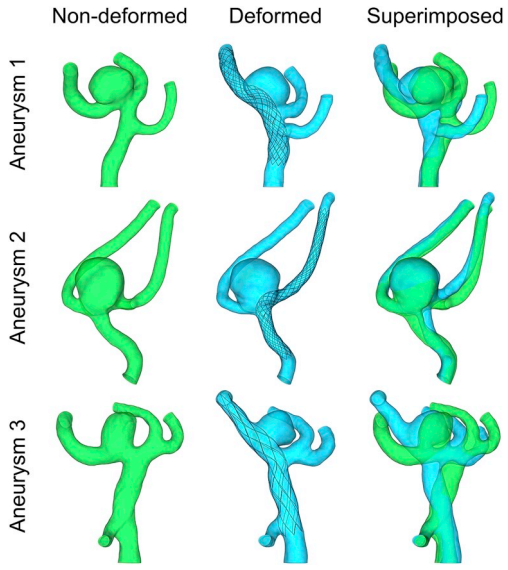

Fig. 2. Visualization of the three considered MCA aneurysms in the pre- (green) and post- (blue) interventional configuration. Due to the stent stiffness, a certain degree of permanent vascular deformation is present. Notice that previous studies generally consider the non-deformed configuration for investigating the effect of stents on hemodynamics.

2. Materials and methods

For an improved understanding of the overall workflow, Fig. 1 visualizes the main steps of this study; from the imaging to the analysis of the simulation results. Further details are described in the following subsections.

2.1. Case descriptions

Three patient-specific saccular intracranial aneurysms were included in this study (see Fig. 2). All three aneurysms were located at the MCA bifurcation, showing a maximum diameter of approximately 6 mm, 9 mm, and 6 mm for aneurysm 1, 2, and 3, respectively. According to Chau et al. [6], vessels at this site are the most likely to deform. The 3D rotational angiographies were acquired on an Artis Q (Siemens Healthineers, Forchheim, Germany). The time between image acquisitions of both states was 177 days, 28 days, and 93 days, respectively. According to the authors' experience (and no contrary reports), the follow-up image is considered representative of the final deformation. Therefore, the permanent deformation (instead of the temporary deformation during the interventions) is captured. For every aneurysm, different configurations were modeled in this study: a) the initial and the post-interventional morphology, b) with and without stent deployment, and c) with and without coil placement. All possible combinations led to eight configurations per aneurysm, and thus resulted in a total of 24 unsteady CFD simulations.

2.2. Segmentation

An image dataset for each aneurysm and each state (non-deformed

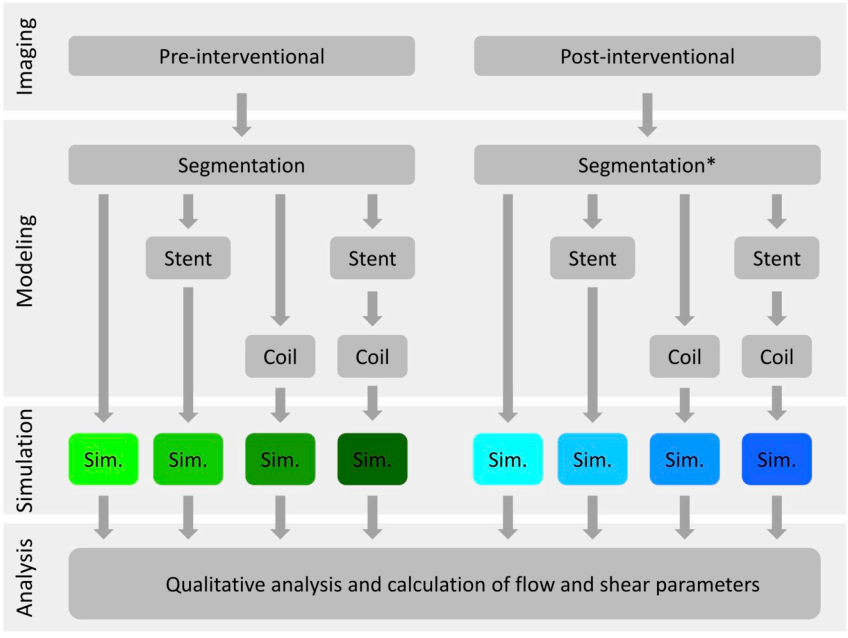

Fig. 1. Workflow of the study: Pre- and post-interventional data sets were segmented. For each case, both segmentations were registered and the coordinate system of the post-interventional state was transformed to match the one of the pre-interventional (*). Due to stent deployment and/or definition of a coil package, eight configurations were created for every patient. The subsequent simulations are color-coded to match the diagrams in Fig. 6.

and deformed) was segmented using MeVisLab 2.8 (MeVis Medical Solutions AG, Bremen, Germany). With 3D image registration, the post-interventional state was transferred to the coordinate system of the pre-interventional state. Due to successful treatment in the follow-up image however, only small amounts of contrast agent entered each aneurysm, resulting in a very limited representation of the aneurysm in the post-interventional state. Nevertheless, the position of the aneurysm was evident due to a) the visible coil package, b) a contrast filled aneurysm neck, and c) small amounts of contrast agent inside the aneurysm sac. Based on these landmarks, the aneurysm geometry from the pre-interventional state was transferred and positioned to the post-interventional configuration. A similar procedure was described in Refs. [19,20]. Finally, plausibility was confirmed by an experienced neuroradiologist.

2.3. Vessel curvature calculation

The vessel deformation due to the stent's stiffness was evaluated based on the centerline of the aneurysm's parent vessel. The Vascular Modeling Toolkit (vmtk) was used to extract the centerlines from the segmentations [21]. A line in space is generally described by its curvature and torsion. The curvature, which is the inverse of the local osculating radius, can adequately quantify the vessel deformation [9]. Thus, after resampling the centerline at a spacing of 0.02 mm, the curvature was calculated using vmtk as well. Finally, the mean curvature and its standard deviation were computed for the centerline section, which was covered by the stent.

2.4. Stenting procedure

Aneurysm 1 and 2 were treated with braided stents (Accero, Acandis GmbH, Pforzheim, Germany) with nominal diameters × lengths of 3 × 20 mm and 2.5 × 20 mm, respectively. Aneurysm 3 was treated with a 3.5 × 20 mm laser-cut stent (Acclino flex, Acandis GmbH, Pforzheim, Germany). Based on the individual stent parameters, the procedure was virtually reproduced using a validated in-house fast virtual stenting approach [22,23]. This comprises a geometric deformation of the nominal stent structures, which is based on the segmented vessel surface and the corresponding vessel centerline. Due to the nature of the approach, clinical applicability is feasible and allows for the reproduction of the real interventions. Furthermore, this methodology retains the true shape of the device and the stent pores were explicitly resolved using a body-fitted mesh. A comparison of the real and virtual stenting results revealed that the start and end positions of the devices were identical.

2.5. Coiling procedure

After stent placement, coiling was performed using Axium (Medtronic plc, Dublin, Ireland) and/or SMART coils (Penumbra Inc., Alameda, California, USA). These coils were not explicitly resolved in the simulation due to the unknown and random location of the single wires. Instead, the theory of porous media was applied to mimic their effect on the hemodynamics [17]. The coil volume divided by the aneurysm volume gives the packing density. This quantity is often used to describe a coiling procedure and is correlated with treatment success. For the porous media definition of the individual coil package specification, two quantities are required: 1) Porosity, which quantifies the occluded aneurysm volume similar to the packing density, and 2) permeability, a measure of the fluid conductivity through the porous medium. Table 1 lists the considered parameters calculated according to Kakalis et al. [24].

2.6. Hemodynamic simulations

Spatial discretization was based on polyhedral cells (base size ranging from 0.085 to 0.115 mm) and five layers of prism cells to resolve the near wall flow. In a previous study mesh-independency requirements were demonstrated for hemodynamic simulations of (treated) intracranial aneurysms [25]. This led to a total number of finite volume cells to be approximately three million (without stent) and approximately eight million (with stent). Blood was assumed to be an incompressible ($\rho = 1055\,\mathrm{kg/m^3}$) and non-Newtonian fluid (*Carreau-Yasuda* model: $\eta_0 = 15.92$ mPa s, $\eta_\infty = 4$ mPa s, $\lambda = 0.08268$ s, $a = 2$, $n = -0.4725$; all parameters were acquired in the local rheology lab).

Table 1
Parameters of the porous media representing the individual coil package.

Aneurysm	Packing density in %	Porosity in %	Permeability in m^2
1	45.5	54.5	2.11E-09
2	43.0	57.0	1.78E-10
3	20.9	79.1	3.32E-08

The mass flow inlet waveform was acquired from a healthy volunteer using 7T phase-contrast MRI [26] and scaled according to Valen-Sendstad et al. [27]. Furthermore, no-slip wall conditions and area-weighted flow-split outlets based on Murray's law [28,29] were applied. In this regard, it must be highlighted that the commonly used zero-pressure assumption for outflow conditions was rejected. Since measurements of the actual pressure variations were not present, the consideration of the aforementioned flow-splitting approach is feasible.

The final 24 configurations were solved using STAR-CCM+ 12.02 (Siemens Product Lifecycle Management Software Inc., Plano, TX, USA) assuming laminar flow conditions. The time-dependent simulations were carried out with a time step of 0.5 ms, i.e., 2000 time steps in a cardiac cycle. Continuity and all three velocity components were chosen as stopping criteria, and residuals of 1E-4 had to be fulfilled in every time-step. In total, three cardiac cycles were calculated for every case; the first two for initialization and obtaining a periodic solution, and the third for the actual post-processing.

2.7. Post-processing

The analysis of the blood flow simulation results focused on four flow and four shear parameters [30]. Regarding the flow description, the following parameters are considered: 1) mean velocity within the aneurysm sac (AV), which represents the temporal and spatially averaged velocity magnitude in each aneurysm, 2) aneurysm neck inflow rate (NIR) quantifying the time averaged blood flow into the aneurysm sac, 3) mean ostium inflow area (OIA), representing the cycle averaged area of entering blood flow, and 4) inflow concentration index (ICI), which evaluates the degree of flow concentration that enters the aneurysm. Equation (1) defines the ICI using the NIR, the flow rate in the parent vessel Q_v, the area of inflow OIA and the total ostium area A_o, respectively.

$$ICI = \frac{NIR/Q_v}{OIA/A_o} \tag{1}$$

Furthermore, the following shear-related parameters are used for analysis: 1) averaged wall shear stress (AWSS), which is the spatial and temporal mean shear value on the corresponding aneurysm, 2) normalized wall shear stress (nAWSS) representing the ratio between shear along the aneurysm surface and the shear distribution at the associated parent vessel, 3) high shear area (HSA), which defines the region of abnormally high shear stress on the aneurysm surface, and 4) shear concentration index (SCI), which is a measure for the degree of concentration of the wall shear stress distribution. In Equation (2), it is defined based on the total viscous shear forces of HSA F_h, the entire aneurysm F_a, and the ratio of HSA to total aneurysm surface area (A_a).

Table 2
Mean and standard deviation of vessel curvature before and after deformation.

Aneurysm	State	Curvature		
		Mean in mm^{-1}	Standard deviation in mm^{-1}	Reduction in %
1	Non-deformed	0.25	0.19	43.7
	Deformed	0.14	0.08	
2	Non-deformed	0.21	0.20	29.2
	Deformed	0.15	0.13	
3	Non-deformed	0.23	0.13	34.9
	Deformed	0.15	0.08	

$$SCI = \frac{F_h/F_a}{HSA/A_a} \quad (1)$$

3. Results

3.1. Vessel curvature

The stent-induced deformation is quantified by means of the local curvature of the vessel centerline. In the pre-interventional state, the mean curvature amounts to 0.21–0.25 1/mm, see Table 2. In the post-interventional state, the curvature is reduced by 43.7%, 29.2%, and 34.9%, for aneurysm 1, 2, and 3, respectively. This corresponds to a straightening of the vasculature in all cases, recall Fig. 2.

3.2. Qualitative hemodynamic results

The qualitative results for aneurysms 1, 2, and, 3 are visualized in Figs. 3–5. Iso-surfaces of the time averaged velocity field indicate the aneurysm inflow jet according to the pre- and post-interventional configurations, and how the flow leads to local AWSS patterns. Qualitative trends due to the impact of deformation, stenting, and coiling are described using aneurysm 3 (see Fig. 5) in the following text: Deformation leads to a redirection of the aneurysm inflow jet, causing a migration of the flow impingement zone from the dome to the neck region. In addition, the transformed hemodynamic conditions inside the aneurysm sac lead to reversed vortices. As a result, the region of high AWSS is shifted close to the neck and the WSS direction at the aneurysm dome is reversed. Stents with high porosity (i.e., low mesh density) hardly affect the intra-aneurysmal flow, but they do alter the WSS in the parent vessel. However, as expected, coils decrease the overall neck inflow velocity and lead to generally reduced WSS on the aneurysm sacs.

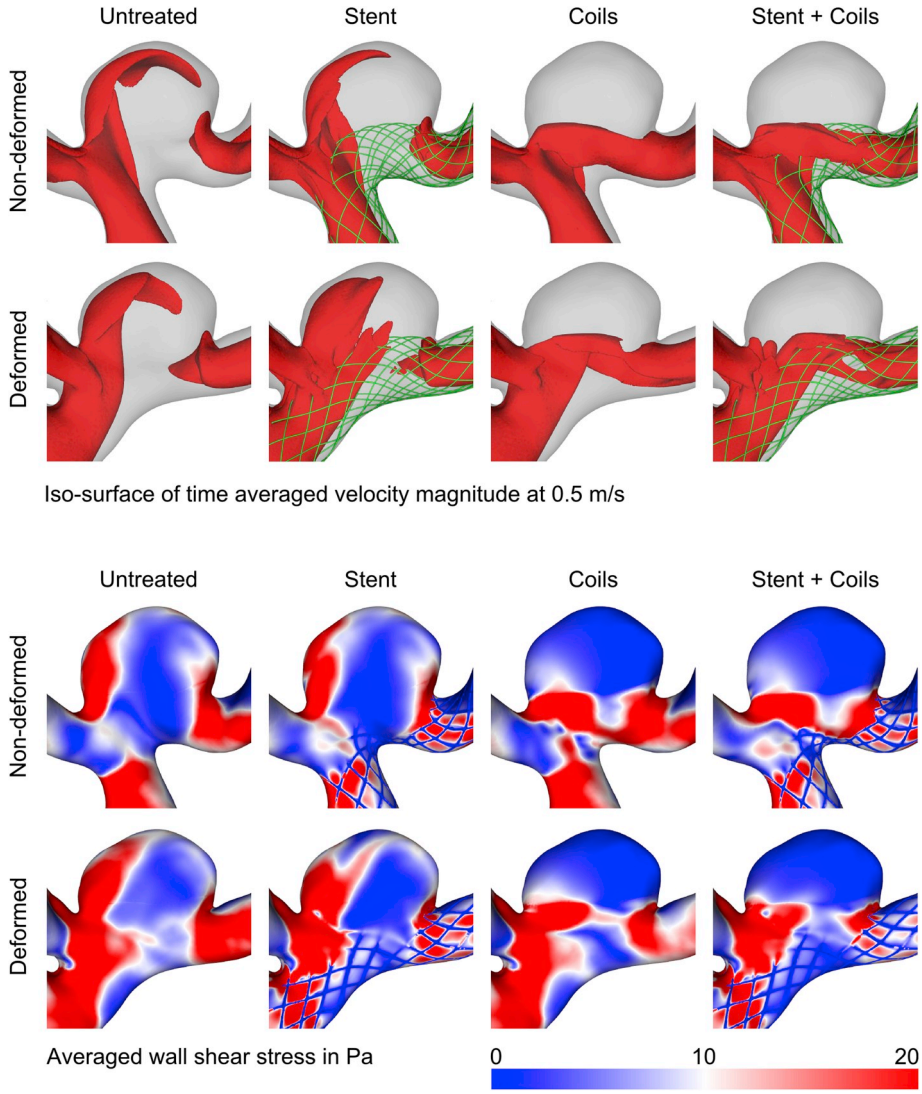

Fig. 3. Qualitative hemodynamic results of aneurysm 1: Velocity iso-surfaces (top) visualize the averaged flow patterns inside the aneurysm, which affect the local AWSS (bottom).

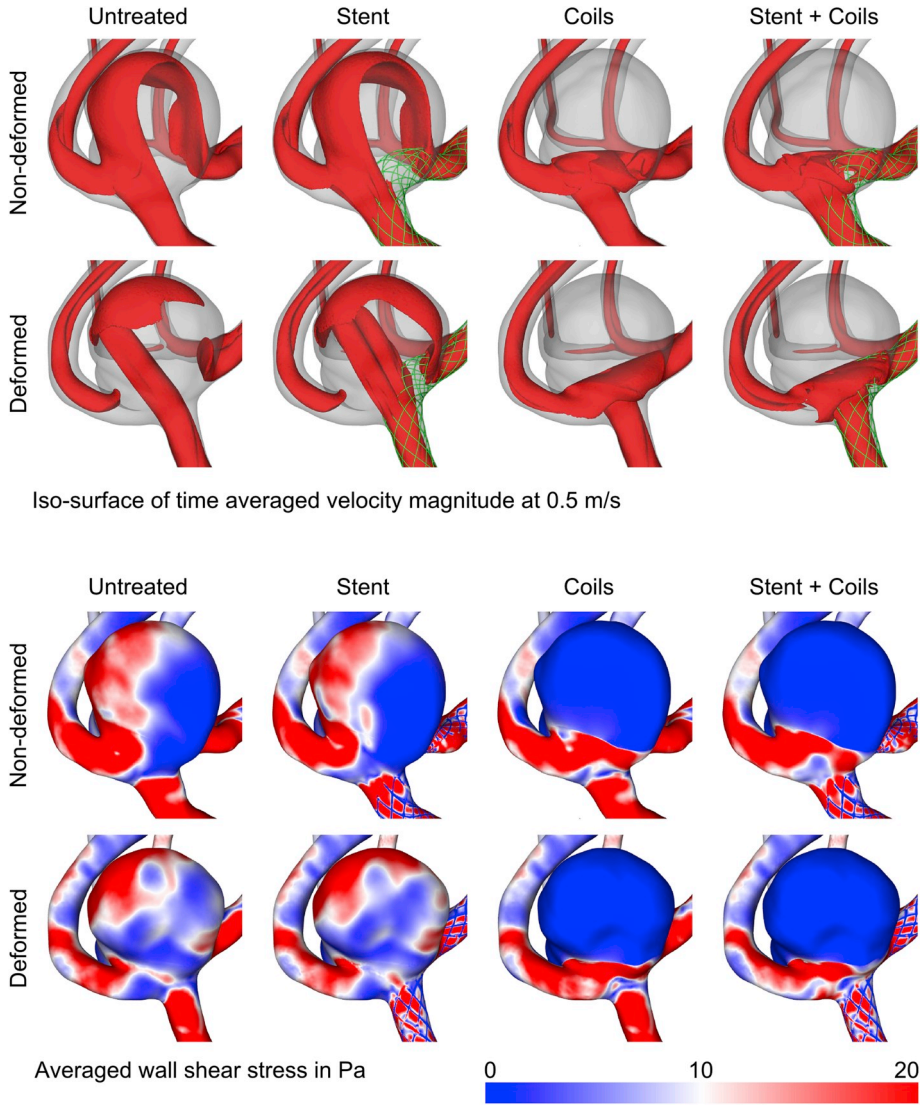

Fig. 4. Qualitative hemodynamics results of aneurysm 2: Velocity iso-surfaces (top) visualize the averaged flow patterns inside the aneurysm, which affect the local AWSS (bottom).

3.3. Quantitative hemodynamic results

Bar plots in Fig. 6 show flow (top) as well as shear (bottom) parameters for each of the three aneurysms. Relative differences of the bar plots are given in Table 3. Regarding the deformation, the impact on flow parameters is inconsistent among the aneurysms. In aneurysms 1 and 2, deformation increases AV by 12.1% and 12.7%, respectively, and NIR by 7.3%, while ICI remains almost constant (-2.1% and -2.4%). Aneurysm 3 experiences a curvature reduction of 34.9%, causing a large inflow jet migration and an observable decrease of AV by 33.9%, NIR by 48.1%, and ICI by 51.5%. The OIA is less affected by the deformation (maximum of 12.2%). It differs in both the area value and location within the ostium (see Fig. 5), e.g., the altered location of the inflow jet at the ostium level in Fig. 5 left, non-deformed versus deformed. Furthermore, changes in AWSS and nAWSS reflect the behavior of AV and NIR; if the inflow jet is redirected from the aneurysm dome, the WSS decreases and vice versa. Due to jet redirection, deformation leads to modifications of the SCI and HSA as well. Moreover, deformation associated detachment of the inflow jet of aneurysm 2 (see Fig. 4) leads to a fivefold increase of HSA. Overall, vascular deformation can cause conflicting outcomes with respect to the different aneurysms.

Stent or coil placement leads to more consistent findings regarding the flow and shear parameters. A stent with low flow resistance has a minor impact on the investigated parameters, except for nAWSS and HSA. With respect to these quantities, the stent struts decrease the blood velocity near the vessel walls. Therefore, the WSS of the parent artery is reduced, which increases nAWSS accordingly (maximum 67.8% for aneurysm 1). In addition, the stent struts near the ostium disturb the inflow jet, decreasing the local impulse on the wall. As a result, HSA is reduced by 25.4% to up to 43.5% in the aneurysms.

Coiling has the strongest impact on the flow behavior, but this clearly depends on the coil packing density. High packing densities in aneurysm 1 (45%) and 2 (43%) lead to a decrease of AV by 89.5% and 98.9%, and of NIR by 75.0% and 95.4%, respectively. Aneurysm 3 had the lowest packing density (21%), and therefore deformation dominates the parameter reduction; particularly with respect to NIR (48.1% over 10.8% due to coils) and ICI (51.5% over 1.2%). Shear parameters are even more affected by the presence of coils. AWSS and nAWSS are reduced by more than 60%, and HSA by more than 90%. Regarding SCI, the results differ: As only low shear is exerted on the wall of aneurysm 2 and distributed homogeneously after coiling, no WSS peaks are present, resulting in a SCI of zero.

The sum of all effects represents the true post-interventional

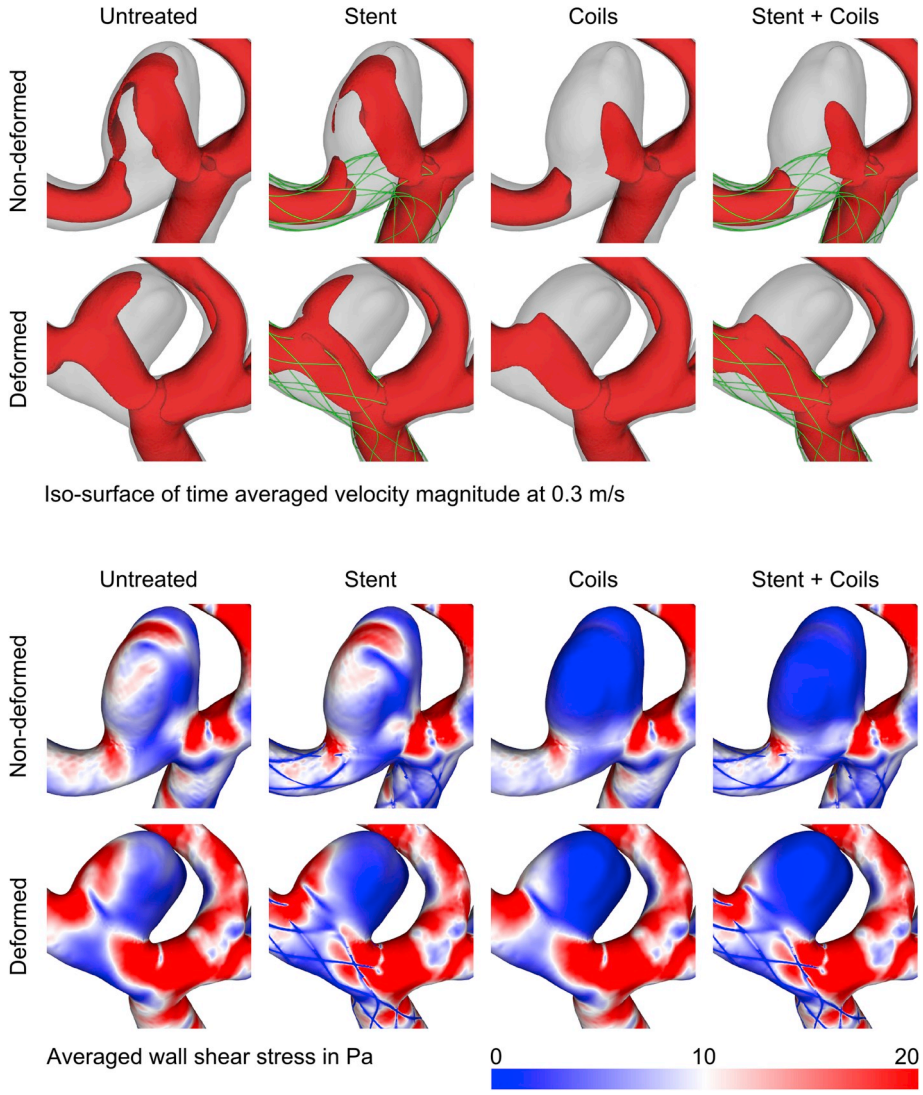

Fig. 5. Qualitative hemodynamic results of aneurysm 3: Velocity iso-surfaces (top) visualize the averaged flow patterns inside the aneurysm, which affect the local AWSS (bottom).

configuration (deformed with stent and coils). Comparing the sum to the single effect results, the coiling effect led to fewer differences between the pre-treated and post-treated geometries for aneurysm 1 and 2. This is different in the case of aneurysm 3. The largest deformation in combination with lowest packing density causes deformation as the primary effect.

4. Discussion

Stent-assisted coiling is an established treatment procedure for intracranial aneurysms, but morbidity and mortality are relatively high at 5% [31–33]. Therefore, virtual techniques are applied to improve the individual treatment outcome and optimize the patient-specific therapy [23,34–36]. Studies of this kind mainly consider the pre-interventional vasculature and apply their virtual treatment to pre-interventional image datasets. However, clinical observations demonstrate that vessel deformations may occur due to treatment [5–10].

To account for this condition, the current study considers vessel deformation and associated differences in blood flow simulation results; see Table 3 (column deformation) or Figs. 3–5 (non-deformed versus deformed state). Therefore, earlier studies may have neglected influences from deformation by this amount. In particular, the combination of lower coil packing densities (moderate inflow rate reduction) and large deformation (distinct inflow redirection) can have a major impact on local flow patterns, and thus have an effect on the shear distribution.

4.1. Individual effects of vessel deformation, stenting and coiling

To address such phenomena, this study evaluates both the individual and combined impact of 1) vessel deformation, 2) stent deployment, and 3) coiling of the aneurysm sac. As the different configurations are based on a virtual experiment, not all of them exist in clinical practice. Regardless of possible intermediate configurations, the initial (non-deformed, without stent and coils) and the post-interventional state (deformed, with stent and coils) are expected to most accurately mirror real-life settings. However, the aim of this study was to determine the effect of each individual influencing factor on its own, and hence these academic configurations are required.

In the following, all results and comments refer to the cases analyzed only in the frame of this study and should not be considered generalizable: Based on the computational results, it can be noticed that coiling has the strongest immediate effect on the local hemodynamics, and that blood flow is globally reduced, depending on the underlying packing density. Furthermore, stenting (with high porosity) alone has the least amount of influence, as the stent struts represent only small resistance against the initial flow situation. However, the most

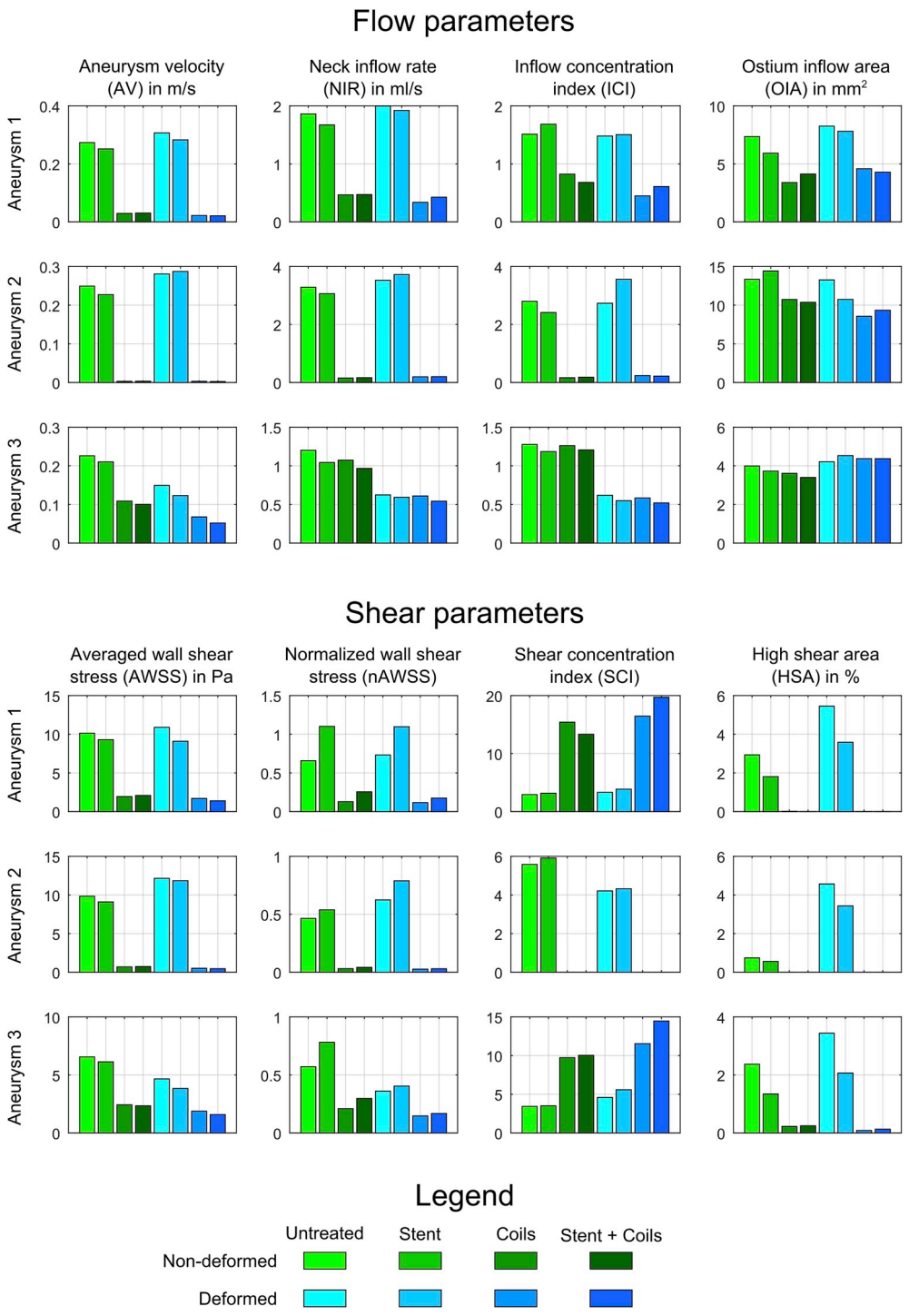

Fig. 6. Bar plots of all three aneurysms - flow parameters: Aneurysm velocity (AV), neck inflow rate (NIR), inflow concentration index (ICI), ostium inflow area (OIA); shear parameters: mean average wall shear stress (AWSS), normalized wall shear stress (nAWSS), shear concentration index (SCI), high shear area (HSA).

interesting observations are possibly due to the treatment-induced vessel deformation. The deformation, quantified by the average centerline curvature, is reduced by between 29.2% (aneurysm 2) and 43.7% (aneurysm 1). As a result, clear changes of flow and shear parameters are evident compared to the pre-interventional state. In particular, this has both positive and negative consequences with respect to hemodynamic parameters, and can lead to either a promotion or an interference of thrombotic processes desired by the treatment. Furthermore, vessel deformation leads to a redirection of the aneurysm inflow jet. Thus, the conditions of local WSS, direction of shear, or oscillatory shear can differ completely from the physiological state. This may have an important effect on the biomechanical properties of the vessel wall.

4.2. *Therapeutic usability of stent-induced vessel deformations*

Considering that deformation can have a major impact on intra-aneurysmal hemodynamics, the question arises whether a therapeutic effect can be caused by the stent alone. On the one hand, the deformation-induced effect is most likely strong enough (e.g., see

Table 3
Deviation of the flow and shear parameters induced by deformation, stent, coils, and combined for the three aneurysms, respectively. The percentage changes refer to the non-deformed untreated configurations. Red panels indicate a relative increase, whereas blue panels refer to a decrease of the corresponding parameter.

	Aneurysm velocity (AV)				Neck inflow rate (NIR)			
Aneurysm	Deformation	Stent	Coils	Sum	Deformation	Stent	Coils	Sum
1	12.1%	-8.1%	-89.5%	-92.5%	7.3%	-10.2%	-75.0%	-77.2%
2	12.7%	-8.8%	-98.9%	-99.0%	7.3%	-6.8%	-95.4%	-94.0%
3	-33.9%	-7.0%	-51.9%	-77.0%	-48.1%	-13.3%	-10.8%	-54.9%

	Inflow concentration index (ICI)				Ostium inflow area (OIA)			
Aneurysm	Deformation	Stent	Coils	Sum	Deformation	Stent	Coils	Sum
1	-2.1%	11.4%	-45.6%	-59.9%	12.2%	-19.5%	-54.0%	-41.8%
2	-2.4%	-13.8%	-94.2%	-92.3%	-0.6%	8.0%	-19.6%	-30.1%
3	-51.5%	-7.2%	-1.2%	-59.3%	5.5%	-6.7%	-9.7%	9.4%

	Averaged wall shear stress (AWSS)				Normalized wall shear stress (nAWSS)			
Aneurysm	Deformation	Stent	Coils	Sum	Deformation	Stent	Coils	Sum
1	7.3%	-8.5%	-81.0%	-86.4%	11.3%	67.8%	-80.7%	-73.6%
2	23.5%	-7.4%	-93.0%	-95.5%	34.3%	15.8%	-93.4%	-93.7%
3	-29.0%	-6.6%	-63.1%	-76.0%	-36.9%	36.9%	-63.4%	-70.8%

	Shear concentration index (SCI)				High shear area (HSA)			
Aneurysm	Deformation	Stent	Coils	Sum	Deformation	Stent	Coils	Sum
1	12.9%	7.1%	425.8%	572.0%	86.0%	-38.3%	-99.6%	-100.0%
2	-24.6%	5.9%	-100.0%	-100.0%	516.4%	-25.4%	-100.0%	-100.0%
3	33.5%	1.9%	183.5%	322.2%	45.1%	-43.5%	-90.7%	-94.6%

aneurysm 3), but on the other hand, the parameter values were not improved in every case (e.g., see aneurysm 2). The effect may need to be enhanced by further increasing the grade of deformation, which correlates to the inflow jet redirection [37]. In the extreme case, it could mean turning a bifurcation into a sidewall aneurysm. However, this has limitations (deformation is constrained by surrounding anatomy and may cause afflictions) and further research would be needed in this area. In the future, patient-specific designed devices may be used to optimize the clinical outcome.

In order to take stent-induced vessel deformation into account and its ensuing effect on the treatment outcome, further simulation tools are required. The virtual placement of stents only in the pre-interventional vasculature may ignore the effect of deformation. The structural simulation of the interaction between the vascular wall and the stent may give a tendency as to how the local flow patterns are altered. This could support the treatment planning, especially in the case of higher deformation probability (less flexible stent design and distal location).

To accomplish this goal however, the acquisition of individual wall information is mandatory. In this regard, improved imaging and segmentation techniques may play a crucial role in obtaining more information on the local wall state. The use of intravascular imaging, especially neurovascular optical coherence tomography, has huge potential to assess local wall thicknesses and inhomogeneities [38]. Only when important factors such as wall thickness [39] and composition are detectable, future simulations can become more patient-specific and reliable. Furthermore, several other aspects in the context of intracranial aneurysm modeling must be carefully carried out [40].

4.3. Limitations

This pilot study has various limitations. First, the number of cases (and therefore the considered treatment scenarios) is too small to derive any generalizable conclusions. However, the objective was the evaluation of separate effects during aneurysm treatment. Therefore, the 24 time-dependent simulations (also containing academic configurations) provide valuable insights into therapy-induced flow modifications.

Second, the processing of the medical images underlies different errors with respect to reconstruction and segmentation algorithms. However, the authors quantified these effects in advance in order to minimize them for the subsequent hemodynamic simulations [41].

Third, the virtual reproduction of the coiling and the fast virtual stenting were based on the assumption of a porous medium [42] and on geometric deformations, respectively. Virtual stenting based on finite element analysis can further improve the reproduction of treatment, but becomes clinically inapplicable as a result. Nevertheless, the approach was validated both in-vitro [22] and in-vivo [34]. Furthermore, the validity of the numerical simulations needs to be demonstrated as several modeling assumptions are involved. In this regard in-vitro [43] and in-vivo [26] studies were carried out in advance.

Finally, all vessel walls were assumed to be rigid and vessel deformation was derived exclusively from follow-up images.

5. Conclusion

This pilot study demonstrates that stent-induced vessel deformation can have a considerable impact on intra-aneurysmal hemodynamics. Three MCA aneurysms were chosen to illustrate how both flow and shear distributions can be influenced due to angular modifications of the vasculature. Furthermore, the individual effects of deformation, stenting, and coiling were separated to highlight the individual importance of each aspect. Coiling and stenting caused a distinct and smaller neck inflow rate, respectively, while the impact of deformation was inconsistent among the aneurysms. Overall, the findings reveal that stent-assisted coiling can lead to an improved hemodynamic situation, but also show that a less than satisfactory flow modification may occur.

Funding

This work was partly funded by the Federal Ministry of Education and Research in Germany within the Research Campus *STIMULATE* (grant number 13GW0095A) and by the European Regional

Development Fund (operation number ZS/2016/04/78123) as part of the initiative “Sachsen-Anhalt WISSENSCHAFT Schwerpunkte”.

Conflicts of interest

None.

Ethics approval

The study was performed in accordance with the guidelines of the local ethics authorities.

References

[1] M. Piotin, R. Blanc, L. Spelle, et al., Stent-assisted coiling of intracranial aneurysms: clinical and angiographic results in 216 consecutive aneurysms, Stroke 41 (1) (2010) 110–115.

[2] N. Chalouhi, P. Jabbour, S. Singhal, et al., Stent-assisted coiling of intracranial aneurysms: predictors of complications, recanalization, and outcome in 508 cases, Stroke 44 (5) (2013) 1348–1353.

[3] Y. Hong, Y.-J. Wang, Z. Deng, et al., Stent-assisted coiling versus coiling in treatment of intracranial aneurysm: a systematic review and meta-analysis, PLoS One 9 (1) (2014) e82311.

[4] K. Aydin, A. Arat, S. Sencer, et al., Stent-assisted coiling of wide-neck intracranial aneurysms using low-profile LEO baby stents: initial and midterm results, Am. J. Neuroradiol. 36 (10) (2015) 1934–1941.

[5] E. Beller, D. Klopp, J. Göttler, et al., Closed-cell stent-assisted coiling of intracranial aneurysms: evaluation of changes in vascular geometry using digital subtraction angiography, PLoS One 11 (4) (2016) e0153403.

[6] Y. Chau, L. Mondot, M. Sachet, et al., Modification of cerebral vascular anatomy induced by Leo stent placement depending on the site of stenting: a series of 102 cases, Interv. Neuroradiol. 22 (6) (2016) 666–673.

[7] B. Gao, M.I. Baharoglu, A.D. Cohen, et al., Stent-assisted coiling of intracranial bifurcation aneurysms leads to immediate and delayed intracranial vascular angle remodeling, Am. J. Neuroradiol. 33 (4) (2012) 649–654.

[8] Q.-H. Huang, Y.-F. Wu, Y. Xu, et al., Vascular geometry change because of endovascular stent placement for anterior communicating artery aneurysms, Am. J. Neuroradiol. 32 (9) (2011) 1721–1725.

[9] R.M. King, J.-Y. Chueh, I.M.J. van der Bom, et al., The effect of intracranial stent implantation on the curvature of the cerebrovasculature, Am. J. Neuroradiol. 33 (9) (2012) 1657–1662.

[10] M. Sağlam, O. Kızılkılıç, V. Anagnostakou, et al., Geometrical characteristics after Y-stenting of the basilar bifurcation, Diagn. Interv. Radiol. 21 (6) (2015) 483–487.

[11] K. Takizawa, K. Schjodt, A. Puntel, et al., Patient-specific computer modeling of blood flow in cerebral arteries with aneurysm and stent, Comput. Mech. 50 (6) (2012) 675–686.

[12] S. Appanaboyina, F. Mut, R. Löhner, et al., Simulation of intracranial aneurysm stenting: techniques and challenges, Comput. Methods Appl. Mech. Eng. 198 (45–46) (2009) 3567–3582.

[13] B. Chung, J.R. Cebral, CFD for evaluation and treatment planning of aneurysms: review of proposed clinical uses and their challenges, Ann. Biomed. Eng. 43 (1) (2015) 122–138.

[14] P. Berg, L. Daróczy, G. Janiga, Virtual stenting for intracranial aneurysms, Computing and Visualization for Intravascular Imaging and Computer-Assisted Stenting, Elsevier, 2017, pp. 371–411.

[15] B. Gao, M.I. Baharoglu, A.D. Cohen, et al., Y-stent coiling of basilar bifurcation aneurysms induces a dynamic angular vascular remodeling with alteration of the apical wall shear stress pattern, Neurosurgery 72 (4) (2013) 617–629 discussion 628-629.

[16] B. Gao, M.I. Baharoglu, A.M. Malek, Angular remodeling in single stent-assisted coiling displaces and attenuates the flow impingement zone at the neck of intracranial bifurcation aneurysms, Neurosurgery 72 (5) (2013) 739–748 discussion 748.

[17] W. Jeong, M.H. Han, K. Rhee, The hemodynamic alterations induced by the vascular angular deformation in stent-assisted coiling of bifurcation aneurysms, Comput. Biol. Med. 53 (2014) 1–8.

[18] S. Voß, P. Berg, G. Janiga, et al., Variability of intra-aneurysmal hemodynamics caused by stent-induced vessel deformation, Current Directions in Biomedical Engineering 3 (2) (2017) 305–308.

[19] K. Kono, A. Shintani, T. Terada, Hemodynamic effects of stent struts versus straightening of vessels in stent-assisted coil embolization for sidewall cerebral aneurysms, PLoS One 9 (9) (2014) e108033.

[20] J. Liu, L. Jing, C. Wang, et al., Effect of hemodynamics on outcome of subtotally occluded paraclinoid aneurysms after stent-assisted coil embolization, J. NeuroInterventional Surg. 8 (11) (2016) 1140–1147.

[21] L. Antiga, M. Piccinelli, L. Botti, et al., An image-based modeling framework for patient-specific computational hemodynamics, Med. Biol. Eng. Comput. 46 (11) (2008) 1097–1112.

[22] G. Janiga, C. Rössl, M. Skalej, et al., Realistic virtual intracranial stenting and computational fluid dynamics for treatment analysis, J. Biomech. 46 (1) (2013) 7–12.

[23] G. Janiga, L. Daróczy, P. Berg, et al., An automatic CFD-based flow diverter optimization principle for patient-specific intracranial aneurysms, J. Biomech. 48 (14) (2015) 3846–3852.

[24] N.M.P. Kakalis, A.P. Mitsos, J.V. Byrne, et al., The haemodynamics of endovascular aneurysm treatment: a computational modelling approach for estimating the influence of multiple coil deployment, IEEE Trans. Med. Imaging 27 (6) (2008) 814–824.

[25] G. Janiga, P. Berg, O. Beuing, et al., Recommendations for accurate numerical blood flow simulations of stented intracranial aneurysms, Biomed. Tech. 58 (3) (2013) 303–314.

[26] P. Berg, D. Stucht, G. Janiga, et al., Cerebral blood flow in a healthy Circle of Willis and two intracranial aneurysms: computational fluid dynamics versus four-dimensional phase-contrast magnetic resonance imaging, J. Biomech. Eng. 136 (4) (2014) 41003.

[27] K. Valen-Sendstad, M. Piccinelli, R. KrishnankuttyRema, et al., Estimation of inlet flow rates for image-based aneurysm CFD models: where and how to begin? Ann. Biomed. Eng. 43 (6) (2015) 1422–1431.

[28] C.D. Murray, The physiological principle of minimum work: I. The vascular system and the cost of blood volume, Proc. Natl. Acad. Sci. U. S. A. 12 (3) (1926) 207–214.

[29] C. Chnafa, O. Brina, V.M. Pereira, et al., Better than nothing: a rational approach for minimizing the impact of outflow strategy on cerebrovascular simulations, Am. J. Neuroradiol. 39 (2) (2018) 337–343.

[30] J.R. Cebral, F. Mut, J. Weir, et al., Quantitative characterization of the hemodynamic environment in ruptured and unruptured brain aneurysms, Am. J. Neuroradiol. 32 (1) (2011) 145–151.

[31] W. Brinjikji, M.H. Murad, G. Lanzino, et al., Endovascular treatment of intracranial aneurysms with flow diverters: a meta-analysis, Stroke 44 (2) (2013) 442–447.

[32] W. Brinjikji, G. Lanzino, H.J. Cloft, et al., Risk factors for ischemic complications following pipeline embolization device treatment of intracranial aneurysms: results from the IntrePED study, Am. J. Neuroradiol. 37 (9) (2016) 1673–1678.

[33] D.F. Kallmes, W. Brinjikji, E. Boccardi, et al., Aneurysm study of pipeline in an observational registry (ASPIRe), Interv. Neurol. 5 (1–2) (2016) 89–99.

[34] P. Berg, C. Iosif, S. Ponsonnard, et al., Endothelialization of over- and undersized flow-diverter stents at covered vessel side branches: an in vivo and in silico study, J. Biomech. 49 (1) (2016) 4–12.

[35] D. Ma, T.M. Dumont, H. Kosukegawa, et al., High fidelity virtual stenting (HiFiVS) for intracranial aneurysm flow diversion: in vitro and in silico, Ann. Biomed. Eng. 41 (10) (2013) 2143–2156.

[36] J. Xiang, R.J. Damiano, N. Lin, et al., High-fidelity virtual stenting: modeling of flow diverter deployment for hemodynamic characterization of complex intracranial aneurysms, J. Neurosurg. 123 (4) (2015) 832–840.

[37] S. Voß, P. Saalfeld, S. Saalfeld, et al., Impact of gradual vascular deformations on the intra-aneurysmal hemodynamics, in: A. Maier, T.M. Deserno, H. Handels, et al. (Eds.), Bildverarbeitung für die Medizin 2018, Springer Berlin Heidelberg, Berlin, Heidelberg, 2018, pp. 359–364.

[38] M.J. Gounis, G.J. Ughi, M. Marosfoi, et al., Intravascular optical coherence tomography for neurointerventional surgery, Stroke 50 (2019) 218–223.

[39] S. Voß, S. Glaßer, T. Hoffmann, et al., Fluid-structure simulations of a ruptured intracranial aneurysm: constant versus patient-specific wall thickness, Comput. Math. Methods Med. 2016 (2016) 9854539.

[40] P. Berg, S. Saalfeld, S. Voß, et al., A review on the reliability of hemodynamic modeling in intracranial aneurysms - why CFD alone cannot solve the equation, Neurosurg. Focus (2019), https://doi.org/10.3171/2019.4.FOCUS19181 (in press).

[41] P. Berg, S. Saalfeld, S. Voß, et al., Does the DSA reconstruction kernel affect hemodynamic predictions in intracranial aneurysms? An analysis of geometry and blood flow variations, J. NeuroInterventional Surg. 10 (3) (2018) 290–296.

[42] M.R. Levitt, M.C. Barbour, S. Du Rolland Roscoat, et al., Computational fluid dynamics of cerebral aneurysm coiling using high-resolution and high-energy synchrotron X-ray microtomography: comparison with the homogeneous porous medium approach, J. NeuroInterventional Surg. 9 (8) (2017) 777–782.

[43] C. Roloff, D. Stucht, O. Beuing, et al., Comparison of intracranial aneurysm flow quantification techniques: standard PIV vs stereoscopic PIV vs tomographic PIV vs phase-contrast MRI vs CFD, J. NeuroInterventional Surg. 11 (3) (2019) 275–282.